Negative magnetoresistance in boron-doped nanocrystalline diamond films

B. L. Willems, G. Zhang, J. Vanacken, V. V. Moshchalkov, S. D. Janssens et al.

Citation: J. Appl. Phys. **106**, 033711 (2009); doi: 10.1063/1.3195045
View online: http://dx.doi.org/10.1063/1.3195045
View Table of Contents: http://jap.aip.org/resource/1/JAPIAU/v106/i3
Published by the American Institute of Physics.

Negative magnetoresistance in boron-doped nanocrystalline diamond films

B. L. Willems,[1,a)] G. Zhang,[1] J. Vanacken,[1] V. V. Moshchalkov,[1] S. D. Janssens,[2] O. A. Williams,[2,3] K. Haenen,[2,3] and P. Wagner[2,3]
[1]*Institute for Nanoscale Physics and Chemistry (INPAC), Katholieke Universiteit Leuven, Celestijnenlaan 200D, Leuven B-3001, Belgium*
[2]*Institute for Materials Research (IMO), Hasselt University, BE-3590 Diepenbeek, Belgium*
[3]*Division IMOMEC, IMEC vzw, Wetenschapspark 1, BE-3590 Diepenbeek, Belgium*

(Received 23 April 2009; accepted 8 July 2009; published online 14 August 2009)

We report on the observation of a negative magnetoresistance (NMR) regime in boron-doped nanocrystalline diamond films at low temperatures. A comparative analysis of our experimental results and those reported for systems composed of superconducting granules embedded in an insulating matrix (also referred as granular films) suggest the presence of superconducting regions inside the insulating films as causing the NMR. By considering the latter scenario, the experimental observations are explained by modeling the systems as consisting of a distribution of superconducting granules whose global properties are tuned by the intergrain distance.
 [DOI: 10.1063/1.3195045]

I. INTRODUCTION

Due to its outstanding electronic, mechanical, and thermal properties, diamond became a potential candidate for developing electronic devices which could meet the increasing demand[1] for smallness, higher performance, less power consumption, and heat dissipation. Furthermore, the material rigidity and electrochemical robustness are of interest for high temperature electronic application such as diamond transistors[2] that could operate at $T > 700$ K. In addition, diamond has also shown to have a wide branch of technological applications in optics, tribology, acoustics, and biology. For more details, the reader is referred to Williams *et al.*[3]

Recently, the observation of a negative magnetoresistance (NMR) regime in highly nitrogen-doped (*n*-type) ultrananocrystallite-diamond (UNCD) films has been reported.[4] By considering the system as being a disordered metal, the NMR was attributed to magnetic Aharonov–Bohm[5] phase breaking processes which delocalize carriers trapped by weak localization (WL) effects.[4] This interpretation is based on two observations: (1) the conductivity of the samples shows a weak dependence on the temperature and (2) since the activation energy (E_A), extracted from the Arrhenius plot of the zero-field transport data, continuously diminishes and is everywhere smaller than the thermal energy (k_BT) between 440 and 90 K, it is assumed to be smaller than k_BT at all temperatures. Therefore, transport processes are claimed not to be of the activated type, but characteristic of a disordered metal instead.[4]

However, the experimental data in Ref. 4 have also been shown to fit a strong localized scenario. In fact, Choy *et al.*[6] reinterpreted these results by considering variable hopping range processes as the main mechanism for the electrical transport. For the latter, a coherent interference can occur between the forward scattered paths an electron can take when hopping between two impurities,[7,8] and, as a consequence of that, the system's resistance increases. Similar to the case of WL, the effect of an applied magnetic field is to suppress the coherence by imposing a face difference between the possible paths an electron can take.[7,8] Based on these findings, Choy *et al.*[6] predicted the resistance to vary with field as $\ln(R) \sim \sqrt{B}$, a dependence shown by the $R(B)$ data in Ref. 4. Moreover, the observed weak positive magnetoresistance (PMR) for low fields is attributed to perturbation effects.[6]

Both interpretations are, however, based on the observation of the phenomenon on one single sample. Furthermore, the experimental results presented in Ref. 4 are not conclusive to rule out a single scenario in favor of the other and hence the question about the exact mechanism behind the NMR in UNCD remains open.

Here, we report on the NMR regime observed in boron-doped nanocrystalline diamond (NCD) films. The samples are located in the vicinity of the metal insulator transition (MIT) which is driven by increasing the boron concentration n_B. The evolution of the sample resistance as a function of the temperature and applied magnetic fields, $R_{sq}(T)$ and $R_{sq}(B)$, respectively, supports the presence of nonpercolating superconducting clusters as causing the NMR. A comparative analysis of our results and the data presented in Refs. 4 and 6 suggest the same scenario for explaining the NMR observed in the UNCD films,[4] with the implication that the latter might become superconducting for sufficiently high doping levels.

II. EXPERIMENTAL

NCD films were grown on insulating quartz substrates in a microwave plasma enhanced chemical vapor deposition (CVD) reactor. A H_2/CH_4 plasma was used with methane concentrations below 3%, pressures around 30 Torr, and a temperature[3,9] of 700 °C. Boron doping was mainly controlled by adding trimethylboron (TMB) to the gas phase, with TMB/CH_4 ratios up to 8000 ppm. Structural characterization was performed by scanning electron microscopy

[a)]Electronic mail: bram.willems@fys.kuleuven.be.

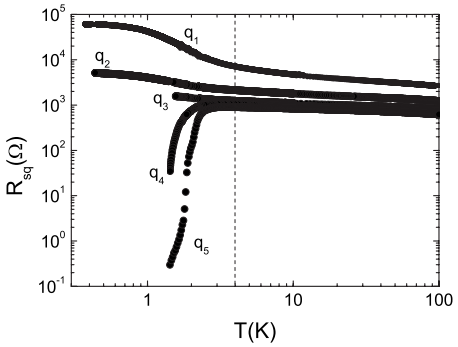

FIG. 1. The temperature dependence of the resistance of the boron-doped diamond films grown on quartz plotted on a log-log scale. The samples differ from each other in their boron concentration, which increases when going from q_1 to q_5. The T_C of q_4 and q_5 are 1.8 and 2.2 K, respectively.

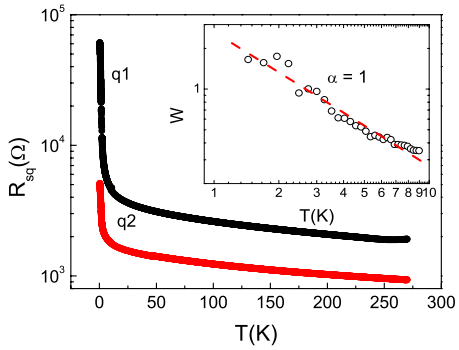

FIG. 2. (Color online) The log-linear plot of the $R(T)$ of samples q_1 and q_2. Inset: The $W=d\ln\sigma/d\ln T$ vs temperature (T) plot of q_1 on a log-log scale. Here, σ is the sample conductivity. The dashed line corresponds to the linear fit.

(SEM) and cross-sectional SEM imaging, as well as by x-ray diffraction (XRD) analysis. Electrical transport properties were probed by using a four-terminal configuration with the contact silver pasted to the corners of the 1×1 cm^2 square samples. Current is caused to flow along one edge of the sample while the voltage was measured between the extremities of the opposite edge. We have found that the resistance measured by using this configuration (which we will label as R_{sq}) showed almost no difference with the obtained when a transport bridge was patterned on one of the samples. The latter evidences the absence of important current redistribution processes in the whole temperature and field range, and hence the sample's extrinsic (resistance) and intrinsic (resistivity) parameters only differ by a constant. The temperatures between 272 and 1.5 K were obtained in an Oxford ^{4}He cryostat. This setup is provided with a 12 T dc magnet coil and a Lakeshore temperature controller. Four-point resistivity measurements were performed with a nanovoltmeter (Hewlett-Packard 34420A) and a programmable current source (Keithley 220). To eliminate thermal or offset voltages while using the nanovoltmeter, the measured voltage is averaged over both positive and negative polarities of the injected current. Typically a current of 10 μA is used. On the other hand, the temperature range between 1.6 and 0.4 K was studied in a Heliox ^{3}He cryostat by Oxford, provided with a 5 T dc magnet coil and a Lakeshore temperature controller as well. In this setup, the sample's resistance was measured by lock in techniques. Typically, the values for the current and frequency were 10 μA and 77 Hz, respectively. In all measurements, fields were applied perpendicular to the sample surface.

III. RESULTS AND DISCUSSION

A. Temperature dependence of the resistance $R_{sq}(T)$

Figure 1 shows the temperature dependence of the sample's resistance $[R_{sq}(T)]$ measured from 100 K. The transport properties of the samples showing a more significant NMR, q_1 and q_2, were additionally explored in the Heliox setup at temperatures down to 0.4 K. The $R_{sq}(T)$ characteristics shown in Fig. 1 are similar to those obtained for granular films consisting of metallic granules embedded in an insulating matrix. In these, the MIT is tuned by the intergrain distance.[10–12] Moreover, the samples lying on the metallic side of the MIT show a state of global superconductivity once the granules are sufficiently close to each other so that the Josephson coupling between them provides the percolating superconducting paths.[13] Previous transport studies performed on a set of NCD samples grown under similar conditions and in the same CVD reactor as the ones presented here, and whose boron concentration n_B was obtained by secondary ion mass spectroscopy analysis,[14] confirm that the MIT observed in Fig. 1 is driven by varying the boron concentration n_B. In other words, n_B increases when going from sample q_1 to q_5. Moreover, since the samples show similar structural characteristics when studied with SEM and XRD, n_B can be considered as the main parameter differing between them.

The $R_{sq}(T)$ dependencies of the samples show similar evolution upon lowering the temperature until approximately 4 K (see Fig. 1). Below this temperature, an important departure, either upward or downward, is observed in the resistance of the samples located at the extremities of the MIT. Furthermore, samples q_4 and q_5 show broad transitions in temperature ($\Delta T>1.5$ K) toward a state of zero resistance, a characteristic for granular superconductivity.[10–13] Their critical temperatures T_C have been found to be 1.8 and 2.2 K, respectively, when taking the criterion of the half value of their normal state resistance. On the other hand, a NMR regime has been observed for the samples which do not show a global superconducting state. In particular, this regime becomes significant in the insulating films q_1 and q_2 of Fig. 1. Therefore, in what follows, the discussion will be focused on the transport properties of these two samples.

Figure 2 shows the zero-field $R_{sq}(T)$ dependencies of both samples. Between 270 and 10 K, the resistance values have increased by more than 100%, becoming more significant between 10 and 1 K with variations $\Delta R>150\%$ and $\Delta R>750\%$ for q_2 and q_1, respectively. Such huge variations over a decade of temperature cannot be attributed to WL effects, for which a $\Delta R<10\%$ is normally expected.[15] Therefore, the transport behavior shown by the samples is of the activated type. Hence,

$$R_{sq}(T)=R_0\exp\{(T_0/T)^{\alpha}\}, \tag{1}$$

with α and R_0 constants. By replotting the zero-field $R_{sq}(T)$ dependencies as $\ln(R_{sq})$ versus $T^{-\alpha}$, good fits were obtained

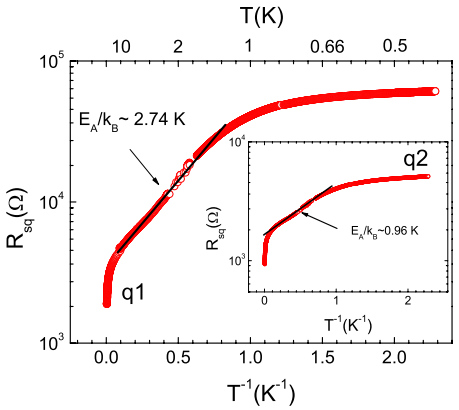

FIG. 3. (Color online) The Arrhenius plots of samples q_1 and q_2 (inset). Good linear fits were obtained in the temperature range between 20 and 1.2 K.

for $\alpha=1$, i.e., transport mainly occurs by nearest neighbor hopping (NNH) processes. The latter is shown in Fig. 3, from which the extracted values for E_A/k_B in the temperature range between 20 and 1.2 K are 2.74 and 0.96 K for samples q_1 and q_2 (inset), respectively. An additional support for the NNH as the main mechanism for the electrical transport is obtaining $\alpha=1$ when replotting the transport data into the more convenient $W=d\ln(\sigma)/d\ln(T)$ versus T dependence on a log-log scale.[16] Here, $\sigma=1/\rho\sim 1/R_{sq}$ is the sample conductivity. Such a $W(T)$ plot allows to extract the values for α without performing any preassumption about the transport regime since

$$W=\frac{d\ln\sigma}{d\ln T}=\alpha T_0^{\alpha}T^{-\alpha}. \tag{2}$$

This is shown in the inset of Fig. 2, in which the $W(T)$ of q_1 is plotted.

B. Field dependence of the resistance $R_{sq}(B)$

Upon increasing the applied magnetic field, samples q_1 and q_2 show PMR→NMR→PMR crossovers. These can be seen in Figs. 4 and 5 where the resistances of q_1 and q_2, respectively, are plotted as a function of the applied magnetic field B. To distinguish between the two PMR regimes, the first will be referred as PMR1 (low field) while the recovered for high fields as PMR2. Figures 4 and 5 show the same features upon lowering the temperature, namely, an increase in both PMR1 and NMR signals, as well as in the values for the field at which the PMR2 is recovered. Moreover, q_1 shows a reduction in its resistance of ΔR 38% at 0.41 K in the NMR region up to the largest attainable field for the setup used. No signs of transition toward PMR2 is observed for 5 T, indicating a larger value in percentage for the total variation ΔR. On the other hand, the negative ΔR is about 26% for q_2 at 0.5 K. Correlations with the transport data (Fig. 2) show a clear correspondence between the negative ΔR and the increase in $R_{sq}(T)$ upon lowering the temperature: the more significant the latter is, the higher values for ΔR and the higher the temperature is at which the NMR is manifested. The crossover from NMR to PMR2 at high fields

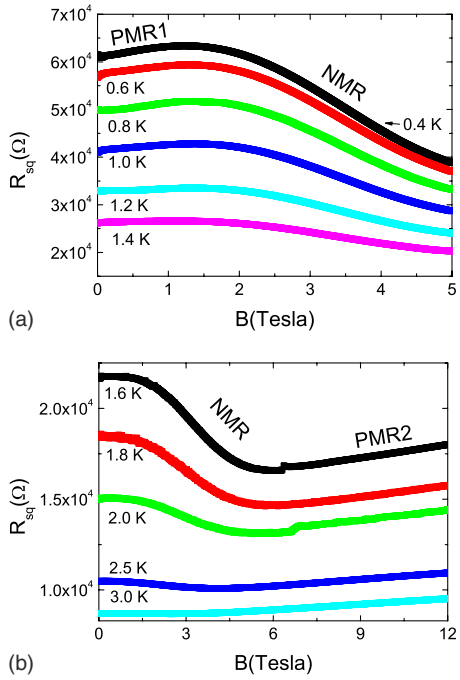

FIG. 4. (Color online) The magnetoresistance of sample q_1 for temperatures between (a) 0.4 and 1.4 K and (b) 1.6 and 3 K. NMR stands for negative magnetoresistance.

can be attributed to orbital shrinking processes which decouple overlapped wave functions between impurities.[17]

Finally, PMR1 is particularly large for q_2, with a positive $\Delta R\sim 20\%$ at the lowest measured temperature (see Fig. 5). Moreover, the positive increase in $R_{sq}(B)$ becomes steeper upon lowering the temperature and survives for fields as high as 1.4 T for $T=0.5$ K. On the other hand, PMR1 in q_1 is resolved at lower temperatures when compared to q_2 (1.4 K versus 1.6 K). Furthermore, the increment in the resistance is about 4% at 0.4 K but it survives above 1 T, similar to the case of q_2.

C. Discussion

Besides having similar transport characteristics as those of granular films showing a MIT,[10–12] the $R_{sq}(T)$'s of the NCD samples at the extremities of the transition experience important deviations around 4 K (Fig. 1). We have to remark that in granular films, Cooper pairs have been found to be present on both insulating and superconducting sides of the

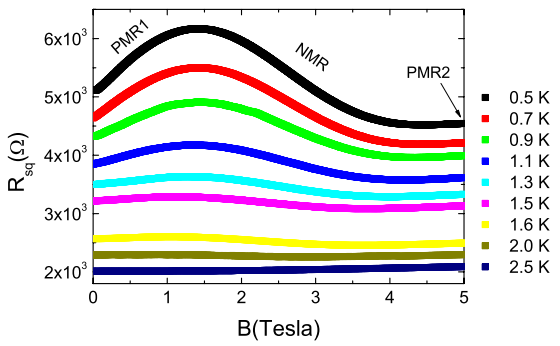

FIG. 5. (Color online) The magnetoresistance for sample q_2 measured between 0.5 and 2.5 K. NMR stands for negative magnetoresistance.

MIT.[18,19] Moreover, these appear at the T_C corresponding to the bulk value[18,19] and are evidenced by the onset of the resistance decrease/increase in the $R(T)$ curves at this temperature. On the other hand, the samples studied here revealed a granular morphology when viewed under SEM, from which crystallite granules are resolved[3,9] with an average size of 400 nm. Moreover, scanning tunneling microscopy (STM) studies performed on superconducting NCD films grown on Si substrates show that these possess an intrinsic granularity, evidenced by the variation in the superconducting gap over a length scale much smaller than the structural grain size.[20] The similarities between the transport properties of granular films and boron-doped NCD, as well as the extrinsic and intrinsic granularities revealed by the latter, suggest the presence of nonpercolating superconducting regions in the insulating samples q_1 and q_2.

Upon increasing the boron concentration (see Fig. 1), the films show a crossover from a strongly localized regime, in which transport occurs through hopping processes, toward a state of a disordered metal. By modeling the samples as an array of superconducting grains embedded in an insulating matrix, the MIT observed in Fig. 1 can then be explained as being driven by tuning the granule/matrix volume ratio V_g/V_{mat}. Hence, the sample is insulating for V_g/V_{mat} smaller than a threshold value, while it shows a state of global superconductivity for the opposite case. Since the number of superconducting granules in a NCD film depends on the number of regions which are optimally doped, i.e., in which the local n_{B} exceeds a critical value[21,22] n_C, the sample's n_{B} is directly correlated with V_g/V_{mat}. The latter scenario allows the presence of superconducting regions in the insulating samples located close to the MIT.

The observation of a PMR1 region in Figs. 4 and 5, together with the reduction in its magnitude when decreasing n_{B}, can be explained by the simple model given above. Since in the vicinity of the MIT an insulator still has a diluted distribution of superconducting grains, some of these will start to become Josephson coupled upon lowering the temperature. The latter leads to the opening of nonpercolating zero-resistance channels and, as a result, the sample conductivity experiences a small but measurable increase below the T_C of the grains. Therefore, when switching on the field, R_{sq} first increases due to the decoupling between the grains (PMR1 in Figs. 4 and 5). Because the n_{B} of sample q_2 is larger than that of q_1, more superconducting grains are expected in the former and hence a more significant PMR1 signal. This is in agreement with the experiment.

On the other hand, NMR regimes were observed in systems consisting of superconducting granules embedded in insulating matrices[23] as well as in superconducting and insulating TiN films located close to the superconductor insulator transition.[24] Moreover, correlations between transport and local spectroscopic properties strongly favor the presence of superconducting regions in the latter.[24] In the granular model described above, the NMR can be understood as follows: for sufficiently high fields Cooper-pair transfer between the superconducting grains is suppressed and single-quasiparticle tunneling settles.[25] The latter implies that the intergrain conductivity will be affected by fluctuations in the density of states (DOS) of the tunneling quasiparticles.[25] Since two quasiparticles are required to form a virtual Cooper pair inside a grain, then the larger the number of the latter the less quasiparticles are available for tunneling.[25] Hence, suppression of the virtual Cooper pairs by further increasing the field is translated into a decrease in the resistance[25] (NMR in Figs. 4 and 5). The fact that the NMR is more significant in q_1 can be attributed to the smaller sizes of the regions that are optimally doped, which is analogous to having smaller superconducting grains. Since fluctuations become more important upon reducing the superconductor size,[26] higher fields are required for destroying the virtual Cooper pairs inside the grains. An additional support for the presence of superconducting fluctuations in the insulating samples is given in Fig. 6. Here, the field values (B_1) at which the crossover between the NMR and the PMR2 happens are plotted as a function of the temperature for sample q_1. It can be seen that these follow a temperature dependence similar to the empirical dependence $B_C \approx B_{C0}[1-(T/T_C)^{1/2}]$ found for the critical field.[27] Moreover, the T_C extracted from this fit is 3.8 K, a value that is consistent with the temperature at which the sample zero-field resistance starts to increase (see Fig. 1). As mentioned before, the recovering of the PMR signal at high fields (PMR2) is attributed to orbital shrinking processes.[17]

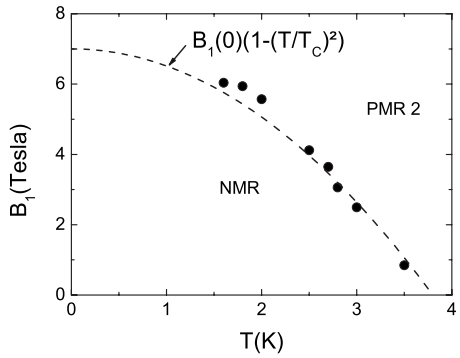

FIG. 6. The temperature dependence of the fields at which the NMR →PMR2 crossover happens for sample q_1. The dashed line corresponds to the fit of the B_1 values by using a temperature dependence similar to that empirically found for the superconducting critical field.

We would like to finalize our discussion with the following remarks. We have found that our data fall within some of the criteria used in Refs. 4 and 6. From the Arrhenius plot of the $R_{\mathrm{sq}}(T)$ dependencies (Fig. 3), the extracted E_A is lower than k_BT over almost all the temperature range. Hence, according to Mareš *et al.*,[4] it should be a disordered metal. However, the NMR signals become more significant for the temperatures below the values for E_A/k_B shown in Fig. 3. Moreover, proceeding likewise with the zero-field resistance values shown in Fig. 2 of Ref. 4, a $E_A/k_B \sim 1.46$ K is obtained and, again, it is below this temperature where the NMR becomes more significant.[4] On the other hand, upon plotting the $R(B)$ data as $\ln(R)$ versus $\sqrt{B}$, we also found a linear dependence for the NMR, in agreement with Choy *et al.*[6] This can be seen in Fig. 7. We have to note here that such a dependence is also expected for three dimensional WL processes.[27] However, neither the WL nor the strong localization scenario accounts for the significant PMR1 responses

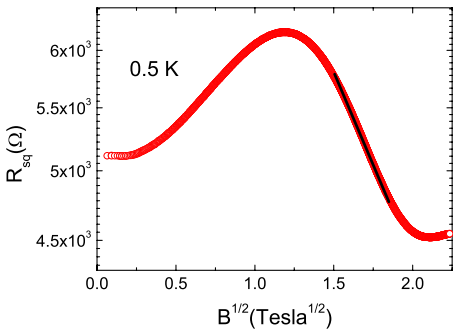

FIG. 7. (Color online) The $R(B)$ data for sample q_2, taken at 0.5 K, plotted as a function of $\sqrt{B}$ on a semilogarithmic scale.

observed in both of our samples. In particular, the PMR1 in q_2 is more or less of the same magnitude as the NMR. Together with the fact that fields above 1 T are not small, the PMR1 observed for q_1 and q_2 cannot be attributed to perturbative effects. Therefore, the presence of superconducting grains (regions) in the insulating NCD films as causing the NMR regimes observed seems to be the most likely scenario for explaining both the temperature and field dependencies presented here. Because of the similarities between the transport behavior of *n*-doped UNCD and *p*-doped NCD, the above analysis, together with the experimental data presented here, leaves the possibility open for the presence of superconducting regions as causing the NMR observed in Ref. 4.

IV. CONCLUSIONS

We report on the observation of a NMR regime in insulating nanocrystalline boron-doped CVD diamond films grown on quartz substrates. This regime shows up at low temperatures and is preceded by a significant PMR dependence. Our experimental data suggest for the presence of noncoupled superconducting regions (grains) as causing the NMR. Moreover, due to the similarities with the transport behavior of *n*-doped UNCD, the NMR regime observed in the latter might be caused by the same mechanisms. This implies for the possibility of observing a superconducting transition in nitrogen-doped UNCD once an optimum level is achieved.

ACKNOWLEDGMENTS

This work was supported by the European Science Foundation (ESF), NES programme, the Methusalem Funding of the Flemish Government, the IAP-P6/42 project "Quantum Effects in Clusters and Nanowires," and GOA and FWO (Contract Nos. G.0430.07 and G.0068.07) projects.

[1] M. Stoneham, Nature Mater. **3**, 3 (2004).
[2] H. Ye, N. Tumilty, M. Bevilacqua, S. Curat, M. Nesladek, B. Bazin, P. Bergonzo, and R. B. Jackman, J. Appl. Phys. **103**, 054503 (2008).
[3] O. A. Williams, M. Nesladek, M. Daenen, S. Michaelson, A. Hoffman, E. Osawa, K. Haenen, and R. B. Jackman, Diamond Relat. Mater. **17**, 1080 (2008).
[4] J. J. Mareš, P. Hubík, J. Krištofik, D. Kindl, M. Fanta, M. Nesládek, O. Williams, and D. M. Gruen, Appl. Phys. Lett. **88**, 092107 (2006).
[5] Y. Aharonov and D. Bohm, Phys. Rev. **115**, 485 (1959).
[6] T. C. Choy, A. M. Stoneham, M. Ortuño, and A. M. Somoza, Appl. Phys. Lett. **92**, 012120 (2008).
[7] V. L. Nguyen, B. Z. Spivak, and E. Shklovskii, Pis'ma Zh. Eksp. Teor. Fiz. **41**, 35 (1985) [JETP Lett. **41**, 42 (1985)];Zh. Eksp. Teor. Fiz. **89**, 11 (1985) [Sov. Phys. JETP **62**, 1021 (1985)].
[8] B. I. Shklovskii and B. Z. Spivak, in *Hopping and Related Phenomena*, edited by H. Fritzsche and M. Pollack (World Scientific, Singapore, 1990), p. 139.
[9] O. A. Williams, O. Douhéret, M. Daenen, K. Haenen, E. Osawa, and M. Takahashi, Chem. Phys. Lett. **4457**, 255 (2007).
[10] H. M. Jaeger, D. B. Haviland, B. G. Orr, and A. M. Goldman, Phys. Rev. B **40**, 182 (1989).
[11] Y. Shapira and G. Deutscher, Phys. Rev. B **27**, 4463 (1983).
[12] K. Kagawa, K. Inagaki, and S. Tanda, Phys. Rev. B **53**, R2979 (1996).
[13] C. A. M. dos Santos, C. J. V. Oliveira, M. S. da Luz, A. D. Bortolozo, M. J. R. Sandim, and A. J. S. Machado, Phys. Rev. B **74**, 184526 (2006).
[14] W. Gajewski, P. Achatz, O. A. Williams, K. Haenen, E. Bustarret, M. Stutzmann, and J. A. Garrido, Phys. Rev. B **79**, 045206 (2009).
[15] S. Kobayashi, in *Localization, Interaction, and Transport Phenomena*, edited by B. Kramer, G. Bergmann, and Y. Bruynseraede (Springer-Verlag, Berlin, 1985), p. 18.
[16] T. Tshepe, C. Kasl, J. F. Prins, and M. J. R. Hoch, Phys. Rev. B **70**, 245107 (2004).
[17] B. I. Shklovskii and A. L. Efros, in *Electronic Properties of Doped Semiconductors*, Springer Series in Solid-State Sciences Vol. 45 (Springer-Verlag, Berlin, 1984).
[18] M. A. Paalanen, A. F. Hebard, and R. R. Ruel, Phys. Rev. Lett. **69**, 1604 (1992).
[19] Y. M. Strelniker, A. Frydman, and S. Havlin, Phys. Rev. B **76**, 224528 (2007).
[20] B. L. Willems, V. H. Dao, J. Vanacken, L. F. Chibotaru, V. V. Moshchalkov, I. Guillamön, H. Suderow, S. Vieira, S. D. Janssens, O. A. Williams, K. Haenen, and P. Wagner (unpublished).
[21] For the case of diamond films prepared by chemical vapor deposition (CVD) methods, the experimental values for n_C have been found to be between (Refs. 14 and 22) 2×10^{20} and 4.5×10^{20} cm^{-3}.
[22] T. Klein, P. Achatz, J. Kacmarcik, C. Marcenat, F. Gustafsson, J. Marcus, E. Bustarret, J. Pernot, F. Omnes, B. E. Sernelius, C. Persson, A. Ferreira da Silva, and C. Cytermann, Phys. Rev. B **75**, 165313 (2007).
[23] A. Gerber, A. Milner, G. Deutscher, M. Karpovsky, and A. Gladkikh, Phys. Rev. Lett. **78**, 4277 (1997).
[24] T. I. Baturina, A. Yu. Mironov, V. M. Vinokur, M. R. Baklanov, and C. Strunk, Phys. Rev. Lett. **99**, 257003 (2007); B. Sacépé, C. Chapelier, T. I. Baturina, V. M. Vinokur, M. R. Baklanov, and M. Sanquer, *ibid.* **101**, 157006 (2008).
[25] I. S. Beloborodov and K. B. Efetov, Phys. Rev. Lett. **82**, 3332 (1999).
[26] M. Tinkham, *Introduction to Superconductivity* (McGraw-Hill, Singapore, 1996).
[27] A. A. Abrikosov, *Fundamentals of the Theory of Metals* (North-Holland, Amsterdam, 1988).